Analysis of the interplay of protein biogenesis factors at the ribosome exit site reveals new role for NAC

Yvonne Nyathi and Martin R. Pool

Faculty of Life Sciences, University of Manchester, Manchester M13 9PT, England, UK

The ribosome exit site is a focal point for the interaction of protein-biogenesis factors that guide the fate of nascent polypeptides. These factors include chaperones such as NAC, N-terminal-modifying enzymes like Methionine aminopeptidase (MetAP), and the signal recognition particle (SRP), which targets secretory and membrane proteins to the ER. These factors potentially compete with one another in the short time-window when the nascent chain first emerges at the exit site, suggesting a need for regulation. Here, we show that MetAP contacts the ribosome at the universal adaptor site where it is adjacent to the α subunit of NAC. SRP is also known to contact the ribosome at this site. In the absence of NAC, MetAP and SRP antagonize each other, indicating a novel role for NAC in regulating the access of MetAP and SRP to the ribosome. NAC also functions in SRP-dependent targeting and helps to protect substrates from aggregation before translocation.

Introduction

Ribosomes are universal cellular machines that decode mRNA in a vectorial manner to synthesize proteins. During translation, the nascent polypeptide chain moves from the peptidyl-transferase center through the exit tunnel to the exit site, located at the surface of the large ribosomal subunit (Nissen et al., 2000). There, the nascent chain emerges from the ribosome and engages a suite of protein biogenesis factors, which cotranslationally regulate enzymatic processing, folding, and subcellular targeting of the newly made protein (Preissler and Deuerling, 2012; Gloge et al., 2014). The ribosome itself acts as a binding platform for these factors, positioning them for optimal interaction with the nascent chain. Different nascent chains interact with distinct factors, and several of these factors appear to have potentially overlapping binding sites on the ribosome, hence careful regulation of their binding is required for efficient protein biogenesis (Leidig et al., 2013; Pechmann et al., 2013).

The mechanism of translation initiation dictates that all proteins possess a methionine as the first amino acid residue. For the majority of cytosolic proteins, this methionine is removed cotranslationally by the enzyme MetAP (Jackson and Hunter, 1970). However, not all proteins are substrates for MetAP; only those with a small amino acid side chain at the second (P2) residue have their methionine cleaved (Huang et al., 1987; Boissel et al., 1988). After methionine removal, the exposed P2 residue can be further processed by either *N*-myristoyl or *N*-acetyl transferases (Martinez et al., 2008; Starheim et al., 2012).

Eukaryotes possess two distinct cytosolic MetAPs with overlapping specificity (Li and Chang, 1995). In yeast, simultaneous deletion of both isoforms is lethal, indicating an essential role for MetAP (Li and Chang, 1995).

Secretory proteins possess hydrophobic signal sequences that are recognized cotranslationally by SRP (Akopian et al., 2013; Nyathi et al., 2013). Eukaryotic SRP is a ribonucleoprotein particle composed of six proteins and the SRP RNA. SRP binds to the ribosome at the exit site, such that the SRP54 protein, which binds the signal sequence, contacts ribosomal proteins Rpl25 and Rpl35 (uL23 and uL29, respectively, according to new nomenclature; Ban et al., 2014), as well as elements of the 26S rRNA (Halic et al., 2004). SRP54 is optimally positioned to bind a signal sequence as it emerges from the ribosome. Multiple nascent chain-binding factors also contact Rpl25/35, hence it has been termed the universal adaptor site (UAS; Halic and Beckmann, 2005).

Once bound to SRP, the ribosome-nascent chain (RNC)–SRP complex is targeted to the ER membrane via the interaction of SRP with its membrane-associated SRP receptor (SR; Gilmore et al., 1982). SR catalyzes the transfer of the RNC from SRP to the Sec61 complex. Sec61 also binds to the ribosome at the exit site, such that the exit tunnel and the pore of the Sec61 channel are coaligned (Becker et al., 2009; Voorhees et

Correspondence to Martin R. Pool: martin.r.pool@manchester.ac.uk

Abbreviations used in this paper: DSS, disuccinimidyl suberate; GMBS, *N*-(γ-maleimidobutyryloxy)succinimide ester; MBS, m-maleimidobenzoyl-*N*-hydroxysuccinimide ester; MetAP, methionine aminopeptidase; NAC, nascent polypeptide chain–associated complex; RAC, ribosome-associated complex; RNC, ribosome nascent chain; SRP, signal recognition particle; UAS, universal adaptor site.

The Rockefeller University Press $30.00
J. Cell Biol. Vol. 210 No. 2 287–301
www.jcb.org/cgi/doi/10.1083/jcb.201410086

al., 2014). Thus, as the nascent chain extends, it moves through the pore of the Sec61 channel into the ER lumen.

In addition to SRP and MetAP, the nascent polypeptide-associated complex (NAC) also binds close to the exit site where it contacts nascent chains (Wegrzyn et al., 2006; Pech et al., 2010; Zhang et al., 2012). In yeast, NAC exists predominantly as a heterodimer of αNAC (Egd2) and βNAC (Egd1; Reimann et al., 1999), although homodimers of Egd2 and the minor βNAC homologue Btt1 have been reported (Panasenko et al., 2006; del Alamo et al., 2011). NAC has been proposed to play a role in regulating the specificity of SRP substrate binding (Powers and Walter, 1996; del Alamo et al., 2011) and in the delivery of the nascent chain to SRP in vitro (Zhang et al., 2012). However, direct evidence for a role of NAC in ER targeting in vivo is presently lacking. NAC was also shown to collaborate with the ribosome-bound Hsp70, Ssb1/2 in the biogenesis of ribosomal proteins and biogenesis factors (Koplin et al., 2010). Moreover, a role for NAC in proteostasis and a chaperone-like function is supported by recent studies (Kirstein-Miles et al., 2013).

NAC was shown to interact with very short nascent chains as they emerge from the ribosome (Wiedmann et al., 1994; Jungnickel and Rapoport, 1995). SRP is recruited to the ribosome at nascent chain length of ∼30 residues (Berndt et al., 2009). Similarly, MetAP also acts on short nascent chains (<48 residues; Sandikci et al., 2013). This poses a question as to how the interplay of these potentially competing factors is regulated. We therefore investigated how MetAP interacts with the ribosome and how its binding and function can be influenced by other factors. We show that NAC and Map1, like SRP, both contact the ribosome via Rpl25/35 and that NAC prevents antagonism between SRP and Map1 binding.

Results

Map1 interacts with the ribosome at the UAS

Both isoforms of MetAP (Map1 and Map2) were previously shown to be associated with the ribosome (Vetro and Chang, 2002; Raue et al., 2007). However, the nature of this interaction in vivo was not addressed. We therefore investigated the ribosome interaction of the major yeast isoform, Map1. Ribosomes were isolated from cycloheximide-treated cells by centrifugation. The distribution of Map1 between the ribosome-enriched pellet and supernatant fractions was determined by SDS-PAGE and Western blot (Fig. 1 A). At physiological salt concentration (100 mM potassium acetate) quantitative association of Map1 with ribosomes was observed. Upon treatment with higher salt concentrations (150–250 mM), a proportion of Map1 was recovered in the supernatant fraction. Above 300 mM, Map1 was recovered predominantly in the supernatant fraction, suggesting a salt-sensitive ionic interaction of Map1 with the ribosome.

We next assessed whether the nascent chain was necessary to stabilize Map1 binding to the ribosome by using the conditional *prt1-1* strain. This harbors a mutation in the β subunit (p90) oϕ eIF3; upon shift to 37°C, translation initiation is blocked, leading to an accumulation of nonprogrammed 80S ribosomes lacking nascent chains (Fig. S1 A; Naranda et al., 1994). The ribosome association of Map1 was almost identical when extracts from the *prt1-1* mutant grown at 24°C or shifted to 37°C for 20 min were compared (Fig. 1 B). Furthermore, Map1 from both extracts exhibited a similar degree of salt-sensitivity in the ribosome-binding assays (Fig. 1 C). Hence, Map1 binding appears largely independent of the nascent chain.

We next assessed whether Map1 binds to the ribosome at the UAS. We made use of a yeast strain which expresses a C-terminal Rpl25GFP fusion as the sole copy of Rpl25 (Hurt et al., 1999). The *rpl25GFP* strain was previously shown to be compromised in ribosome binding of SRP and cotranslational targeting in vivo (Dalley et al., 2008). Ribosomes were isolated from cycloheximide-treated WT and *rpl25GFP* strains. A marked reduction in the association of Map1 with the ribosome was observed in the *rpl25GFP* strain (Fig. 1 D). This was not a result of reduced overall levels of Map1 in these cells, as the *rpl25GFP* strain had total amounts of Map1 similar to WT (Fig. 1 D).

Next, total MetAP activity was measured in the three strains using a fluorescent peptide assay (Li et al., 2003). The *Δmap1* control exhibited a statistically significant reduction in MetAP activity to ∼50% of WT levels (Fig. 1 E). Consistent with the reduction in ribosome binding, the *rpl25GFP* mutant showed a significant reduction in MetAP activity, although not as marked as in the *Δmap1* mutant. To confirm these findings, shotgun MS/MS sequencing of proteins from the ribosomal fractions with masses around 25–27 kD obtained from the three strains was performed (Fig. S1 B). In the WT strain, methionine cleavage was efficient; we failed to detect any N termini with an intact methionine and a P2 residue, which was a substrate for MetAP cleavage (Table 1), In contrast, in the *rpl25GFP* strain, N-terminal peptides with an intact methionine were detected for Rpl16A, Rpl16B and Pex19. However, N-terminal processing was not affected for all proteins in this fraction; we failed to detect any unprocessed N-terminal peptides for the other proteins, including Rpl7B and Rpl15A. Hence, Rpl16A, Rpl16B, and Pex19 may be particularly sensitive to the reduced level of Map1 at the ribosome in the *rpl25GFP* strain.

To directly address whether Map1 is bound at the UAS, chemical cross-linking was used to induce covalent linkages between ribosome-bound Map1 and any adjacent proteins. A C-terminally FLAG-tagged variant of Map1, which functionally complemented the strong growth defect of a *Δmap1* strain was used (Fig. S2 A). Using the hetero-bifunctional cross-linker MBS, adducts of ribosome-associated $Map1_{FLAG}$ to partners of 10, 12, 14, 20, and 25 kD were observed (Fig. 1 F). The 12-kD adduct is in good agreement with the size of Rpl35. Furthermore, an identically sized (58-kD) cross-link product, which cross-reacted with Rpl35 antibody, was specifically immunoprecipitated with anti-FLAG antibody (Fig. 1 F). When the cross-link profile of Rpl35 for WT and *Δmap1* ribosome fractions were compared, this 58-kD adduct was specifically absent in the *Δmap1* strain, even on very long film exposures (Fig. S2 B).

Map1 and Map2 have distinct modes of interaction with the ribosome

A *Δmap1* strain is sensitive to the Map2 inhibitor fumagillin as it becomes reliant on Map2 for MetAP activity, unlike a *MAP1* strain, which is completely insensitive (Sin et al., 1997). We noticed that the *rpl25GFP* strain was retarded in growth in the presence of fumagillin (Fig. 2 A), suggesting, that it is dependent on Map2. Hence, Map1 and Map2 may be differentially affected by the *rpl25GFP* fusion.

We therefore compared ribosome association of Map1 and Map2, using an HA-tagged variant of Map2. $Map2_{HA}$ readily associated with ribosomes in WT cells (Fig. 2 B). In contrast to Map1, Map2 binding was unaffected in the *rpl25GFP*

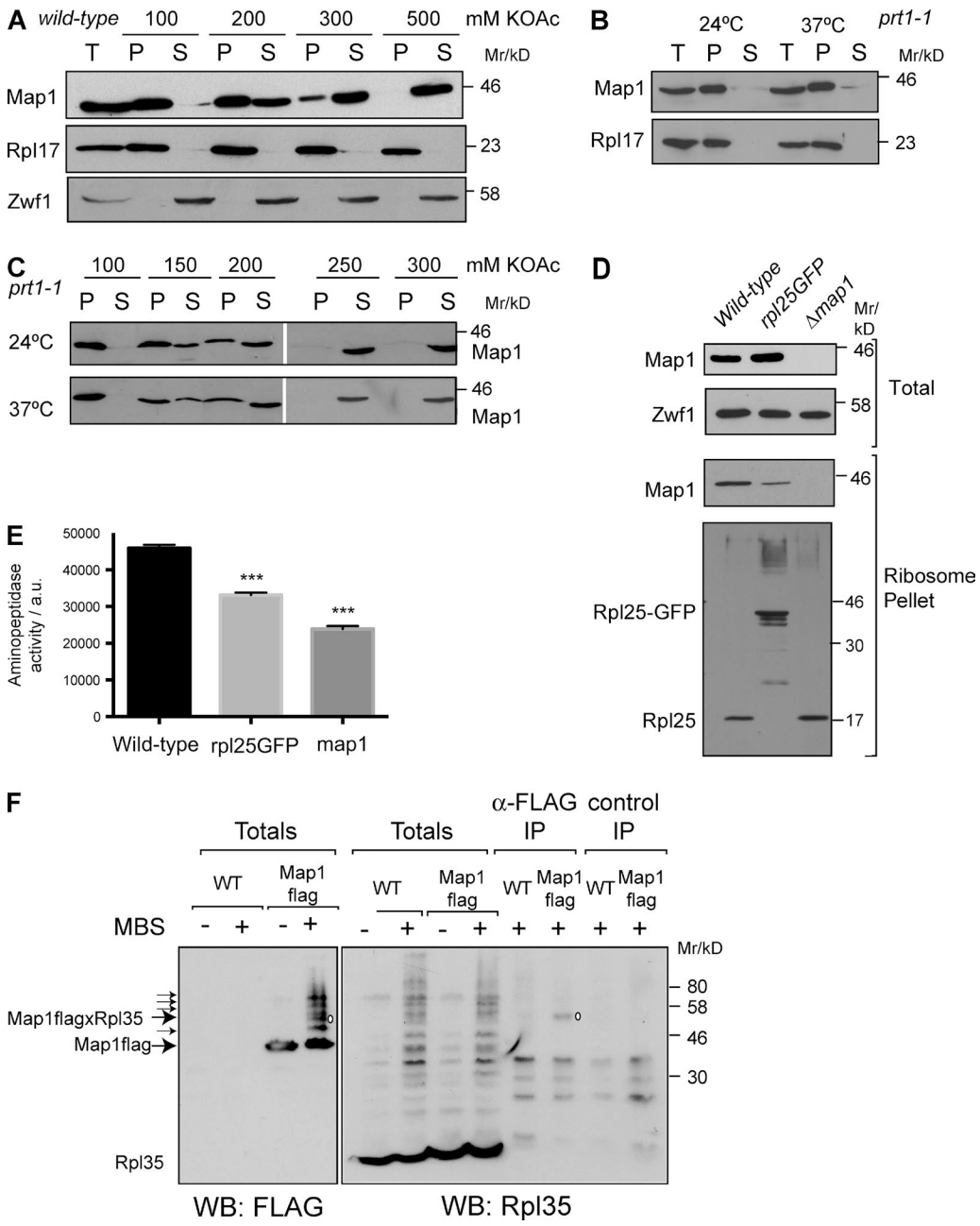

Figure 1. **Association of Map1 with the ribosome at the UAS.** (A) Extracts from WT cells (W303; T), were centrifuged through sucrose cushions at indicated salt concentrations to generate a ribosome-enriched pellet (P) and supernatant fraction (S). Fractions were analyzed by SDS-PAGE and blotting for Map1, Rpl17 (ribosome marker), and Zwf1 (cytosolic marker). (B and C) Ribosome pelleting analysis was performed as in A in the presence of 100 mM (B) or indicated salt concentrations (C) with *prt1-1* (YMK135) cells grown either at 24°C or after a 20-min shift to 37°C followed by blotting for indicated proteins. (D) Ribosome pelleting was performed from WT (RS453), *rpl25GFP* and *Δmap1* (GFY9) strains as in A. Pellets were analyzed by Western blot for Rpl25, Map1, and Zwf1 (loading control). (E) MetAP activity in total lysates from the indicated strains was determined using the fluorogenic substrate Met-AMC, as described in Materials and methods (error bars = SEM; *n* = 3). (F) Ribosome pellets from WT or a *Δmap1::MAP1*$_{FLAG}$ strain (GFY9::pMP289) were cross-linked with 250 μM MBS, followed by denaturing immunoprecipitation with anti-FLAG or control (α-myc) antibodies. Total reactions and immunoprecipitates (IP) were analyzed by Western blot for FLAG or Rpl35. The Map1xRpl35 cross-link is indicated (o).

strain, and was slightly elevated in a *Δmap1* strain (Fig. 2 B). To assess whether Map1 and Map2 have distinct ribosome binding modes, Map1 was overexpressed from the strong *TDH3* promoter. This led to almost stoichiometric binding of Map1 to the ribosome as judged from the Coomassie staining of Map1 to a similar intensity as ribosomal proteins (Fig. 2 C). The cross-linking profile of ribosome-associated Map1 from this strain revealed identical sized adducts to those observed with Map1 at endogenous levels, including the cross-link to Rpl35 (Fig. S2 C), suggesting that overexpressed and endogenous Map1 interact similarly with the ribosome. Despite the dramatically elevated levels of Map1 on the ribosome, there was no reduction in Map2 binding (Fig. 2 C). Conversely, overexpression of Map2 from the *TDH3* promoter led to a dramatic increase in Map2 binding to the ribosome, without affecting Map1 binding (Fig. 2 D). Furthermore, Map1 and Map2 asso-

Table 1. **N-terminal peptides derived from 25–27 kD proteins from a ribosome-enriched fraction from WT (RS453, *RPL25*) and *rpl25GFP* cells (Fig. S1 B)**

Protein	N-terminal peptides	
	RPL25 (WT)	***rpl25GFP***
Rpl7B	Ac-STEKILTPESQLK	
Rpl15A	GAYKYLEELQR	GAYKYLEELQR
Rpl16B	Ac-SQPVVIDAK	Ac-SQPVVIDAK
	SQPVVIDAK	SQPVVIDAK
		MSQPVVIDAK
Rpl16A	Ac-SVEPVVVIDGK	Ac-SVEPVVVIDGK
	SVEPVVVIDGK	SVEPVVVIDGK
		MSVEPVVVIDGK
Pex11	VCDTLVYHPSVTR	VCDTLVYHPSVTR
		MVCDTLVYHPSVTR

ciated with ribosomes with differing salt sensitivities; Map2 was still associated with the ribosome at 500 mM salt, whereas Map1 was predominantly in the supernatant fraction (Fig. 2 E). Collectively, these results indicate that Map1 and Map2 have distinct ribosome binding modes.

Map1 and NAC can bind simultaneously at the UAS

In addition to Rpl35, Map1 was cross-linked to two other proteins of 20 and 25 kD (Fig. 1 F). In strains deleted of NAC, these two cross-links were absent suggesting they may correspond to adducts between Map1 and NAC subunits (Fig. 3 A). The Rpl35 cross-link was also weaker, suggesting NAC may influence positioning of Map1 next to Rpl35. The 25-kD adduct corresponds to the size of αNAC (Egd2). To assess whether this was a cross-link between the two proteins, ribosomes were prepared from WT, Map1-overexpressing, and $Map1_{FLAG}$-expressing strains. Cross-linking with GMBS and blotting for Egd2 revealed, in addition to an Egd1 cross-link adduct, cross-links to a 43-kD adduct, in good agreement with the size of Map1 (Fig. 3 B). Moreover, this 43-kD ad-

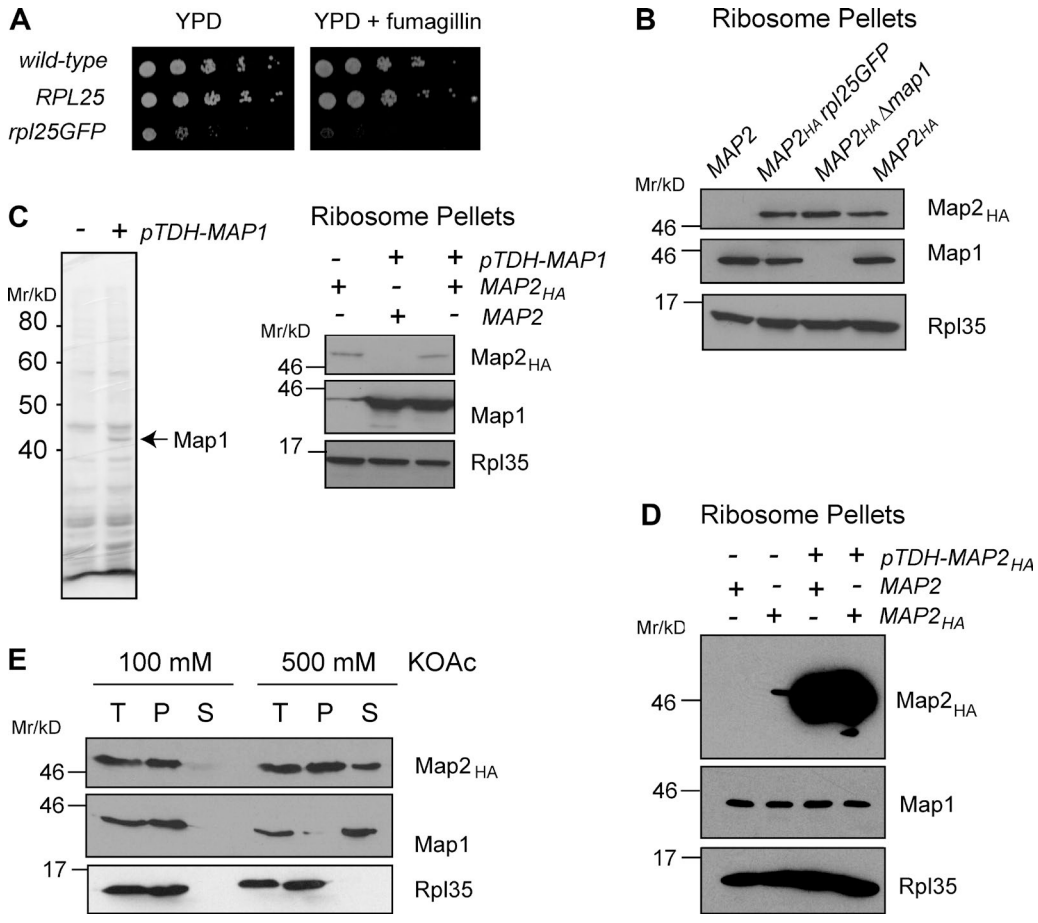

Figure 2. **Map1 and Map2 have distinct interactions with the ribosome**. (A) WT and *Δrpl25* cells complemented with either a plasmid-borne *RPL25 (MPY69)* or *rpl25GFP (rpl25GFP)* were spotted as serial dilutions onto YPD plates with or without 3 µM fumagillin and grown at 30°C for 2 d. (B) Ribosome pellets were prepared from WT (W303), and strains with C-terminally HA-tagged genomic *MAP2 ($MAP2_{HA}$)* W303 *(YNY5)*, *rpl25GFP (YNY3)*, and *Δmap1 (YNY4)* and analyzed by Western blot for HA, Map1 and Rpl35. (C) Ribosome pellets from $MAP2_{HA}$ (YNY5) strain with or without Map1 overexpression plasmid (pTDH-MAP1, pMP299) were analyzed by Western blot for Map2HA, Map1, and Rpl25. The ribosome pellets from WT with (+) and without (–) the pTDH-*MAP1* plasmid were analyzed by SDS-PAGE and Coomassie staining. The position of the Map1 protein is indicated. (D) Ribosome pellets prepared and analyzed as in B from either WT (W303) or $MAP2_{HA}$ (YNY5) strain, transformed with pRS414 (vector) or pMP305 (pGPD-*MAP2HA*). (E) Ribosome pelleting from $MAP2_{HA}$ (YNY5) cell extract was performed in the presence of either 100 mM or 500 mM salt. Resulting total (T), supernatant (S), and pellet (P) fractions were analyzed by blotting for Rpl35, Map2HA, and Map1.

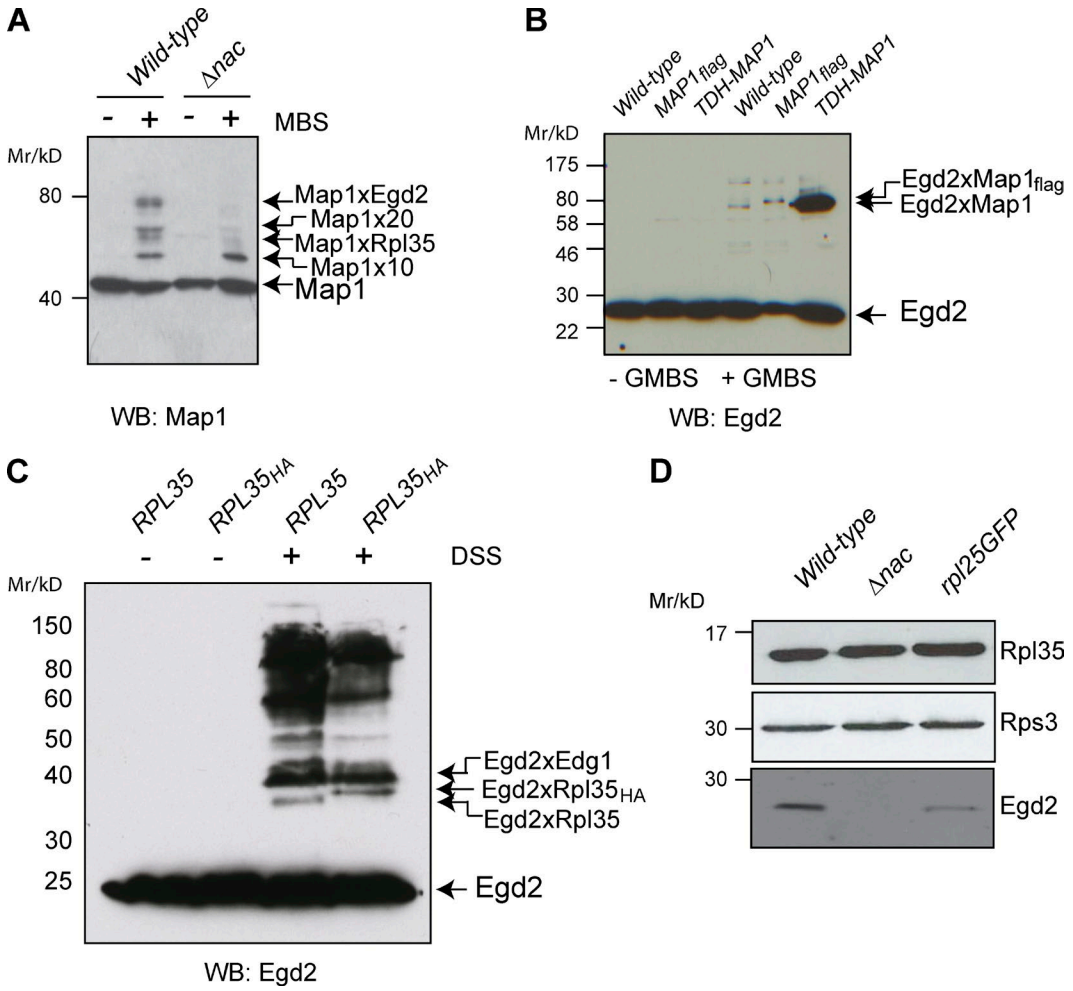

Figure 3. **Map1 is adjacent to NAC at the UAS.** (A) Ribosome fractions derived from WT (BY4741) and *Δnac* strains were treated with the cross-linker GMBS (200 µM) and analyzed by Western blot for Map1. (B) Ribosome fractions from WT yeast (W303) with or without the pTDH-MAP1 plasmid (pMP299), as well a *Δmap1* (GFY9) strain complemented with a $Map1_{FLAG}$ plasmid (pMP289), were treated with GMBS as in A and analyzed by Western blot for Egd2. (C) Cross-linking of ribosome fractions from WT (*RPL35, W303*) and a *Δrpl35A/B* strain expressing a C-terminally HA-tagged *RPL35A* (RBY175) were performed with DSS followed by Western blot for Egd2. (D) Ribosome pellets from indicated strains were analyzed by Western blot for Egd2, Rps3, and Rpl35.

duct was strongly elevated in the Map1 overexpression strain and also shifted upwards in the $Map1_{FLAG}$ strain (Fig. 3 B). Hence, when bound to the exit site, Map1 is positioned close to both Rpl35 and Egd2.

We also assessed whether Egd2 might be positioned close to Rpl35. Indeed, a 12-kD cross-link adduct to Egd2 was observed with the amine-reactive cross-linker DSS, and this was shifted upwards in a strain expressing HA-tagged Rpl35 (Fig. 3 C). The identity of this adduct was confirmed by mass spectrometry of the cross-link product after denaturing immunoprecipitation with anti-HA resin (Fig. S2 D). Moreover, comparison of ribosome pellets of WT and *rpl25GFP* strains revealed a reduction in the levels of Egd2 (Fig. 3 D), thus confirming binding of Egd2 at the UAS.

NAC subunits contact proteins at either side of the ribosome exit site

Egd1 was shown to interact with the ribosome adjacent to Rpl31 (eL31), which is located on the opposite side of the exit site to Rpl35 (Pech et al., 2010; Zhang et al., 2012). To test if this interaction still occurred under the conditions when Egd2 is adjacent to Rpl35, ribosome fractions from an $Egd1_{HA}$ strain were cross-linked using DSS (Fig. S3 A) and cross-link adducts were isolated by denaturing immunoprecipitation using the anti-HA resin. Staining with Coomassie revealed cross-link partners of 10, 25, and 47 kD, which were identified by mass spectrometry as Rpl31, Egd2, and Zuo1, respectively (Fig. S3 B). The Rpl31 and Egd1 adduct is in excellent agreement with previous studies (Pech et al., 2010; Zhang et al., 2012) and Zuo1 is also known to bind to the ribosome close to Rpl31 (Peisker et al., 2008; Leidig et al., 2013). Analysis of the cross-linked MS/MS spectra with MassMatrix (Xu and Freitas, 2009) identified a peptide corresponding to a cross-link between Egd1 lysine 137 and Rpl31 lysine 27 (Fig. S4 B). This maps to the surface-exposed region of Rpl31 (residues 23–41) previously implicated in Egd1 binding (Pech et al., 2010).

Importantly, fusion of the HA-tag to Egd1, did not affect the formation of the Rpl35xEgd2 cross-link (Fig. S3 C). Thus, the previously reported Rpl31–Egd1 interaction could be repro-

duced under conditions whereby Egd2 was detected to be adjacent to both Rpl35 and Map1 by chemical cross-linking.

Interplay of ribosome interaction of NAC, Map1, and SRP

Having established that NAC and Map1, just like SRP54, interact with the ribosome at the UAS, we investigated whether they could influence one another's ribosome binding. The effect of individually overexpressing NAC, Map1, or SRP on the ribosome association of each of the three factors was assessed in a WT strain. Overexpression of SRP led to increased ribosome binding of SRP, but did not alter ribosome-association of NAC or Map1 (Fig. 4 A). Overexpression of Map1 led to increased ribosome binding of Map1 and a low level of Map1 in the supernatant, suggesting that binding was saturated. This had no effect on association of NAC with the ribosome, but led to reduced association of SRP with ribosomes, despite unaltered total cellular SRP levels (Fig. 4 A). Finally, overexpression of NAC led to a modest increase in association of Egd2 with the ribosome and a large pool of Egd2 in the supernatant with no effect on Map1 and SRP ribosome binding (Fig. 4 A).

Overexpression of SRP had a minimal effect on growth rate of a WT strain (Dalley et al., 2008), consistent with the fact that the ribosome association of NAC and Map1 is unaffected (Fig. 4 A). We next investigated the effect of overexpressing SRP in *Δmap1* and *nac* mutants. Overexpression of SRP in a *Δmap1* strain had no effect on growth (Fig. S4 A). In contrast, *Δegd1* mutant overexpressing SRP exhibited a marked reduction in growth, which was further enhanced in a *Δegd1Δbtt1* mutant (Fig. 4 B). The *Δegd2* mutant was also sensitive to SRP overexpression but to a lesser extent than the *Δegd1* (Fig. 4 B and Fig. S4 B).

The association of Map1 in Δegd1 and Δegd2 was investigated using the ribosome-pelleting assay. Upon overexpression of SRP, Map1 was clearly detected in the supernatant fraction (Fig. 4 C). Consistent with this observation, reduced MetAP activity was detected in these mutants using the fluorescent peptide assay (Fig. S4 C).

The fact that in *nac* mutants, Map1 ribosome association was affected upon SRP overexpression led us to ask whether biogenesis of cytosolic proteins might be generally affected in such strains. We therefore investigated whether overexpression of SRP in these strains led to protein aggregation. Overexpression of SRP in a WT strain led to the accumulation of detergent-insoluble aggregates, which were dramatically increased in the Δ*egd1* mutant (Fig. 4 D). The effect was less marked in a Δ*egd2* strain, consistent with the milder growth defect observed in this mutant. The pattern of aggregates observed in a *Δegd1* is similar to that for the *Δssb1/2Δnac* mutant (Fig. 4 D; Koplin et al., 2010), which was enriched in ribosomal and nuclear proteins. Hence, in the absence of NAC, overexpression of SRP can interfere with the biogenesis of nonsecretory proteins.

Overexpression of SRP in the WT led to elevated SRP association with the ribosome (Fig. 4 A). However, a phenotype upon SRP overexpression was only observed in *nac* mutants. To assess whether the overexpressed SRP was bound to the ribosome in an altered manner in Δ*nac* mutants, the cross-linking profile of ribosome-associated Sec65 subunit of SRP was investigated. Strikingly, a strong adduct of 53-kD was observed in WT and *Δegd2* strains but was dramatically reduced in both *Δegd1* and *Δegd1Δbtt1* strains, consistent with the stronger growth defects upon SRP overexpression in these mutants (Fig. S4 D).

To investigate further the interplay of NAC and SRP, ribosome association of SRP in a WT strain and *nac* mutants was compared. SRP association was markedly increased when *EGD1* but not *EGD2* was deleted (Fig. 4 E). This result suggested that Egd1 is important in regulating SRP association with the ribosome. Consistent with this idea, overexpression of Egd1 was accompanied by a growth defect (Fig. S5 A) and a reduction in SRP association with the ribosome (Fig. S5 B). We also monitored cotranslational translocation using a *PHO8-URA3* reporter assay (Dalley et al., 2008). WT cells efficiently target Pho8–Ura3 to the ER and so cannot grow without uracil. Overexpression of Egd1, but not Egd2, led to growth without uracil, indicating a defect in translocation (Fig. S5 C).

NAC is involved in cotranslational translocation

Our data so far support the concept that NAC can prevent the inappropriate interaction of SRP with nonsecretory nascent chains. However, recent studies indicate that NAC can be found associated with a subset of secretory nascent chains (del Alamo et al., 2011) and can facilitate handover of secretory nascent chains to SRP in vitro (Zhang et al., 2012). We therefore revisited any potential role for NAC in cotranslational ER targeting in vivo. It is already known that at 30°C, deletion of NAC subunits does not cause a translocation defect with the sensitive *PHO8-URA3* reporter assay or with Dap2 in a pulse-labeling assay (Dalley et al., 2008; del Alamo et al., 2011). However, when translocation was tested with the *PHO8-URA3* reporter at 16°C, a ura$^+$ phenotype was detected for the *Δegd2* mutant (Fig. 5 A). In contrast, there was no defect detected with a *CPY-URA3* reporter, which exclusively uses the Sec62-dependent targeting pathway (Fig. 5 B; Ng et al., 1996).

To further investigate the potential role of Egd2 in SRP-dependent translocation, we looked for a genetic interaction between Δ*egd2* and a *sec65-1* strain, which has a conditional mutation in the Sec65 subunit of SRP. The *sec65-1* strain grows well at 30°C (Fig. 5 C) but is not viable upon shift to 37°C, where there is almost a complete block in SRP-dependent translocation (Stirling and Hewitt, 1992). At 30°C, the *Δegd2* mutant grew like the WT strain; however, the *sec65-1Δegd2* mutant revealed a marked growth defect (Fig. 5 C).

Using the *PHO8-URA3* reporter, a marked translocation defect was observed in the *sec65-1Δegd2* mutant at 30°C but not in the single mutants (Fig. 5 D). Analysis of total Sec65p levels in the WT, single and double mutants revealed that *sec65-1* cells had lower total SRP levels as well as reduced association of SRP with the ribosome than WT, but this effect was not exacerbated in the *sec65-1Δegd2 mutant*. Hence, an indirect effect of *egd2* deletion on SRP biogenesis can be excluded (Fig. 5 E).

As the presence of Egd2 appears to be important for Pho8 translocation when SRP levels are reduced, we next asked whether elevating Egd2 levels might rescue translocation in a *sec65-1* strain at 37°C. Pulse-labeling of Dap2 revealed an almost complete block in translocation in the *sec65-1* strain after a shift to 37°C, with only the nonglycosylated precursor being detected (Fig. 5 F; Stirling and Hewitt, 1992). In contrast, overexpression of either NAC or Egd2 alone was able to partially restore translocation after a shift to 37°C (Fig. 5 F).

Our observations suggest that Egd2 alone can provide a function in translocation at the ribosome and is positioned at the UAS. However, Egd1 has been proposed to provide

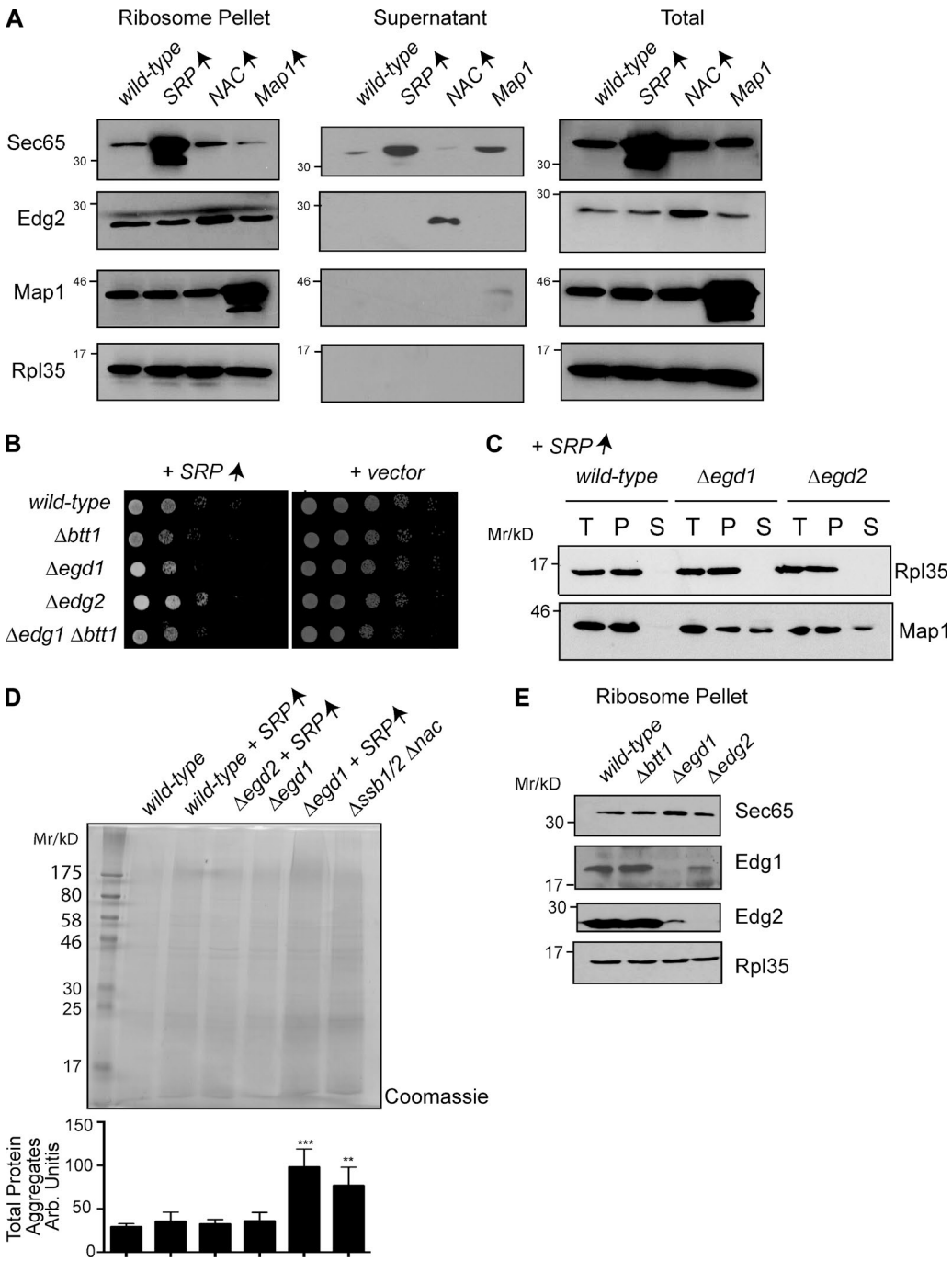

Figure 4. **Interplay of ribosome binding of SRP, NAC, and Map1.** (A) Ribosome pellets, supernatant, and total cell extracts from WT cells, or WT cells transformed with plasmids to overexpress NAC (pMP304), Map1 (pMP299), or SRP (pMW295 and pMW299) were analyzed by Western blot for Sec65, Egd2, Map1, and Rpl35. (B) Serial dilutions of WT strain and the indicated *nac* mutants transformed with SRP overexpression were spotted on −URA/LEU plates and grown at 30°C for 3 d. (C) Ribosomes from WT cells (BY4741), *Δegd1* and *Δegd2* transformed with plasmids overexpressing SRP were analyzed by Western blot for Map1 and Rpl35. (D) WT (BY4741), *Δegd1 and Δegd2* strains transformed with SRP overexpression plasmids or empty vectors and *Δssb1/ssb2Δnac* (control) were grown in minimal medium to mid-log phase. Lysates were extracted with nonionic detergent to yield a pellet enriched in detergent-insoluble aggregates, which were analyzed by SDS-PAGE and Coomassie staining. The amount of aggregates were quantified (error bars = SEM; $n = 3$; **, $P < 0.01$; ***, $P < 0.001$ one-way ANOVA). (E) Ribosome pellets from WT (BY4741), *Δbtt1, Δegd1*, and *Δegd2* cells were analyzed by SDS-PAGE and blotted for Sec65, Egd1, Egd2, and Rpl35.

the major ribosome-binding site for NAC via Rpl31 (Pech et al., 2010; Zhang et al., 2012).

This led us to assess whether Egd2 can still associate with the ribosome in a *Δegd1* strain. Although ribosome binding was reduced, residual binding of Egd2 was still observed. Chemical cross-linking revealed a 52-kD cross-link in this strain, which was also present in a WT strain, albeit at a much reduced level (Fig. S5 D). This cross-link is precisely the correct size for a homodimer of Egd2. Consistent with this, overexpression of Egd2 either alone or together with Egd1 led to elevated association of Egd2 with the ribosome and a marked increase in the 52-kD cross-link product (Fig. 5 G). Furthermore, under

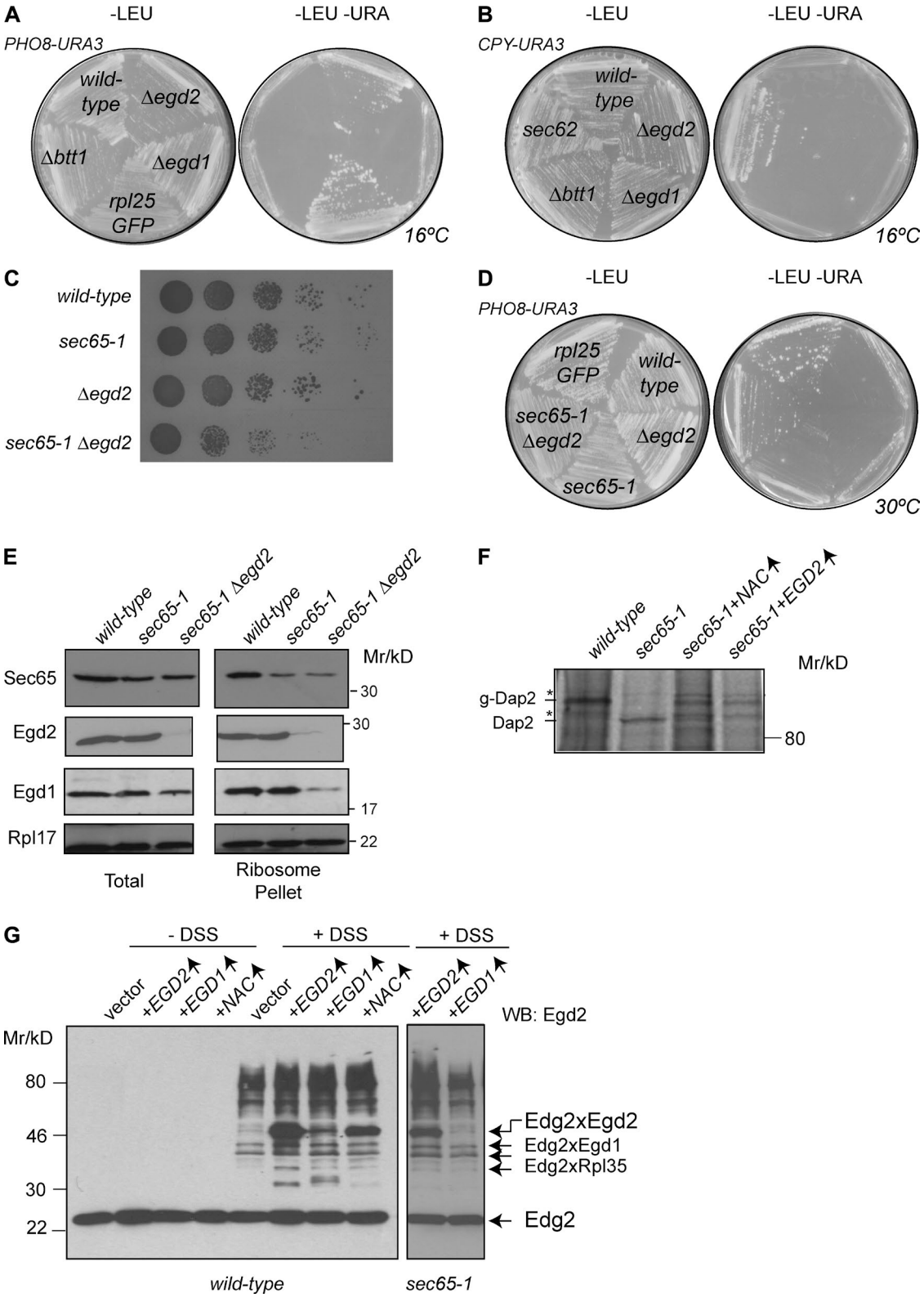

Figure 5. **NAC mutants have mild SRP-dependent translocation defects.** (A) WT (BY4741), *Δegd1*, *Δegd2*, *Δbtt1*, and *rpl25GFP* strains (control) were transformed with a *PHO8-URA3* reporter plasmid *(pMP234)* and streaked onto SD–leu (selects for plasmid) or SD–leu –ura media (selects for translocation defect) and grown for 7 d at 16°C. (B) Translocation assay was performed as in A, but with *CPY-URA3*. (C) WT (W303), *sec65-1 (CSY128)*, *Δegd2*, and *sec65-1Δegd2 (YNY1)* strains were grown to mid-log phase and serial dilutions spotted onto YPD media and grown at 30°C for 3 d. (D) *PHO8-URA3* reporter assay was repeated as in A, but with strains as in C. (E) Total and ribosome fractions from cycloheximide-treated cells for strains as in C were analyzed by Western blot for Sec65, Rpl17, Egd1, and Egd2. (F) Dap2 translocation in WT (W303), *sec65-1 (CSY128)* cells, and *sec65-1* cells overexpressing NAC (pMP304) or Egd2 (pMP302) was analyzed by pulse labeling. Nontranslocated (Dap2) and glycosylated (translocated) forms (g-Dap2) are indicated. (G) Ribosome pellets, prepared from WT and *sec65-1* strains overexpressing Egd1, Egd2, or NAC were treated with DSS and analyzed by blotting for Egd2.

native conditions a similarly sized band was readily detected in strains overexpressing Egd2 or NAC and, to a lesser extent, in WT or with Egd1 overexpression (Fig. S5 E), indicating that this putative Egd2 homodimer is stable in vivo. To confirm that this species is a homodimer, Egd2 was expressed and purified from *Escherichia coli* (Fig. S5 F). Cross-linking of the purified Egd2 with DSS led to the formation of an identical 52-kD cross-link adduct (Fig. S5 F).

EGD2 can prevent aggregation of SRP-dependent translocation substrates

How might Egd2 be acting to rescue translocation in the absence of SRP? We speculated that in this situation, SRP substrates with hydrophobic signal sequences or signal anchors might be prone to aggregation. We therefore investigated whether the *sec65-1* strain accumulates aggregates upon shift to 37°C. At 24°C, WT cells, *Δegd1*, *Δegd2, sec65-1*, and *sec65-1Δegd2* mutants had very low levels of detergent-resistant aggregates (Fig. 6 A). In contrast, upon shift to 37°C, a marked increase in the aggregates was detected only in the *sec65-1* and *sec65-1Δegd2* mutants (Fig. 6 A). To assess whether these aggregates included secretory precursors, Western blot analysis was used to investigate the presence of endogenous Pho8 in the aggregates of the *sec65-1* strain. This was indeed the case, and the *sec65-1Δegd2* strain had a slightly higher level of Pho8 in aggregates (Fig. 6 A). To confirm that the Pho8 detected corresponded to the untranslocated form of the protein, extracts from WT and *sec65-1* cells shifted to 37°C were analyzed by Western blotting for Pho8 (Fig. 6 B). WT total cell extract revealed a single band of Pho8, which was sensitive to PNGase F treatment, indicating that it was N-glycosylated. The *sec65-1* total cell extract revealed a single Pho8 band insensitive to PNGase F treatment, indicating that it was non glycosylated. The detergent-insoluble fraction from WT cells lacked Pho8, whereas the same fraction from *sec65-1* cells contained the PNGase-insensitive species as in the *sec65-1* total cell extract, thus, confirming that the aggregates contain unglycosylated Pho8.

To assess whether these aggregates represented newly synthesized proteins, detergent-insoluble fractions were prepared from the WT, *sec65-1*, and *sec65-1Δegd2* strains after pulse labeling with [^{35}S] methionine and cysteine (Fig. 6 C). WT cells exhibited a very low level of aggregation of radiolabeled newly synthesized proteins in contrast to *sec65-1*, which showed a higher level of aggregation that was further increased in the *sec65-1Δegd2* strain. Thus, the aggregates in the two mutant strains indeed contain newly synthesized protein.

To test if overexpression of Egd2 can suppress aggregation in the *sec65-1* strain and thereby preserve the translocation competence of SRP-dependent precursors, pulse labeling was repeated in the *sec65-1* strain overexpressing Egd2. A marked reduction in aggregation of newly synthesized proteins was observed (Fig. 6 C).

Based on this result, total protein aggregates were examined in *sec65-1* strains overexpressing either NAC or Egd2 from low copy or multicopy plasmids. Consistent with the pulse-labeling result, there was a dramatic reduction of aggregated Pho8 upon expression of either NAC or Egd2 from low copy plasmids which was further reduced with high copy plasmids (Fig. 6 D). Overexpression of either NAC or Egd2 also led to a modest reduction in total aggregated protein.

We noticed that the Pho8 Western blot analysis of the aggregates revealed higher molecular weight species, which is consistent with ubiquitination (Fig. 6 D). Western blot for ubiquitin in the aggregates confirmed a smear of ubiquitinated products, which increased in the *sec65-1Δegd2* strain and was reduced upon expression of Egd2 in the *sec65-1* strain (Fig. 6 E).

Discussion

Map1 is the major isoform of the yeast MetAP. Here, we have shown that when bound to the ribosome, Map1 can be cross-linked to Rpl35. Consistent with this, ribosome-association of Map1 is disrupted by fusion of GFP to Rpl25, which likely sterically hinders access to the UAS, leading to defects in methionine-processing of a subset of cytosolic proteins. We observed a reduction in MetAP activity upon loss of Map1 ribosome association, suggesting that ribosomes may influence the specific-activity of Map1. The positioning of Map1 at the exit site would allow cotranslational processing of the N-terminal methionine as soon as it emerges from the exit site, consistent with previous studies (Jackson and Hunter, 1970). Association of the bacterial MetAP with the ribosome was recently characterized (Sandikci et al., 2013); strikingly, *E. coli* MetAP could also be cross-linked to the bacterial homologue of Rpl25 (uL23), as well as bacterial ribosomal protein bL17, which lacks a direct eukaryotic homologue.

Map1 and Map2 appear to have nonoverlapping ribosome binding sites, indicated by the fact that (a) overexpression of Map1 led to quantitative ribosome binding with no effect on Map2 association, (b) overexpression of Map2 similarly had no effect on ribosome binding of Map1, and (c) the *rpl25GFP* fusion disrupted Map1 binding to the ribosome, but had no effect on Map2.

When bound to the ribosome, Map1 is adjacent to Egd2, and both proteins are close to Rpl35. The fact that we readily detected cross-links between the two proteins indicates that they can bind simultaneously to ribosomes in vivo. Moreover, overexpression of Map1 led to almost stoichiometric occupancy of ribosomes with Map1, with no effect on ribosome association of Egd2 or Egd1. We also detected a cross-link adduct of ∼20 kD to Map1, which was absent in the *nac* mutants. This likely represents a cross-link between Map1 and Egd1. Hence, NAC and Map1 can sit together on the ribosome adjacent to the UAS.

Egd1 was shown to interact with the ribosome via Rpl31 (Pech et al., 2010; Zhang et al., 2012), which is located opposite to Rpl25/35 at the exit site. We also detected cross-links between Egd1 and Rpl31 indicating that Egd2 is adjacent to Rpl35, whereas Egd1 is next to Rpl31. Thus, our data are consistent with previous studies demonstrating interaction at both sites (Wegrzyn et al., 2006; Pech et al., 2010; Zhang et al., 2012). Interestingly, cross-links were detected between Egd1 and Zuo1, which also associates with the ribosome close to Rpl31 (Peisker et al., 2008; Leidig et al., 2013), thereby suggesting that ribosomes can bind NAC and the ribosome–associated complex (RAC) simultaneously.

In contrast to NAC and Map1, which can bind simultaneously to the ribosome, SRP antagonizes ribosome binding of Map1 in the absence of NAC. Ribosomes with both Map1 and NAC bound (upon Map1 overexpression) had reduced interaction with SRP. Overexpression of SRP was tolerated in the presence of NAC, but not NAC deletions, in particular the *egd1* mutant, exhibited growth defects upon overexpression of SRP, which correlated with reduced association of Map1 with the ribosome.

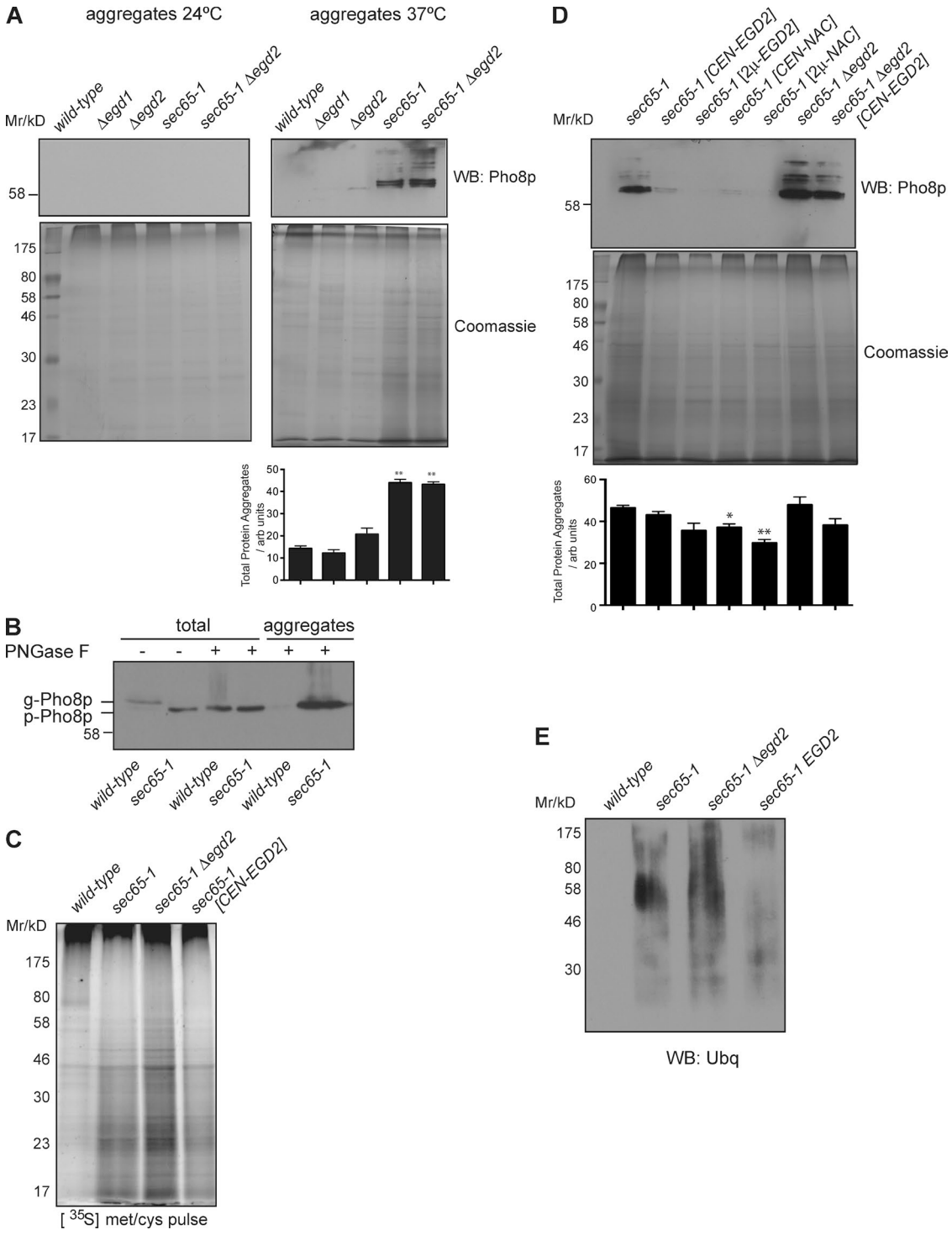

Figure 6. **Egd2 prevents aggregation of nontranslocated SRP-dependent precursors.** (A) WT (W303), *Δegd1*, *Δegd2*, *sec65-1 (CSY128)*, and *sec65-1Δegd2 (YNY1)* strains were grown in YP media at 24°C or shifted to 37°C for 120 min to mid log phase. Lysates were extracted with nonionic detergent to yield a pellet enriched in detergent-insoluble aggregates, and analyzed by SDS-PAGE and Coomassie staining or blotting for Pho8. The total amount of aggregates quantified (error bars = SEM; $n = 3$; *, $P < 0.05$; **, $P < 0.01$ one-way ANOVA). (B) WT (W303) and *sec65-1* (CSY128) strains were grown in YP media to mid-log phase and shifted to 37°C, and aggregates were isolated as in A. Where indicated, extracts were treated with PNGase F. Reactions were analyzed by blotting for Pho8. Position of nonglycosylated (pPho8p) and glycosylated Pho8 (g-Pho8p) is indicated. (C) WT (W303), *sec65-1* (CSY128), and *sec65-1Δegd2* (YNY1) cells were grown to mid-log phase in minimal media at 30°C and then pulse-labeled with [^{35}S] methionine and cysteine for 5 min before analysis as in A but with SDS-PAGE and phosphorimaging. (D) WT (W303) and *sec65-1* (CSY128) harboring CEN or 2 μm plasmids for expressing *EGD1* (pMP300), *EGD2* (pMP301 or pMP302), or NAC (*EGD1* and *EGD2* -pMP303 and pMP304) were analyzed for aggregates as in A. (E) Aggregates from WT, *sec65-1* (CSY128), *sec65-1Δegd2* (YNY1) and *sec65-1* with a CEN *EGD2* plasmid (pMP301) strains were analyzed by blotting for ubiquitin.

In WT cells, both ribosomes and NAC are present in large excess over SRP and Map1 (Raue et al., 2007), hence it is unlikely that SRP and Map1 are simultaneously bound to the same ribosome. This would explain why the absence of NAC has a minimal effect on growth, as the antagonistic effect of SRP on ribosome association of Map1 is limited because of the relatively low concentration of SRP.

The structure of the eukaryotic SRP bound to a secretory RNC indicates multiple contact points, the strongest of which is centered upon Rpl25/35, as well as nearby helix 59 and helix 24 of the rRNA (Halic et al., 2004). We now show that both Map1 and Egd2 can be simultaneously adjacent to Rpl25/35, hence it is perhaps not surprising that all three ligands cannot be accommodated at this site. Consistent with this idea, signal sequences are rarely substrates for Map1 processing (Forte et al., 2011; Sandikci et al., 2013) and N-terminal processing was compromised for an SRP-dependent signal sequence (Forte et al., 2011).

Overexpression of SRP in the *Δegd1* strain led to the accumulation of detergent-insoluble aggregates, which are reminiscent of those observed in a *Δssb1/2Δnac* mutant (Koplin et al., 2010). A previous study showed that *Δnac* mutants display a promiscuous interaction of SRP with cytosolic nascent chains (del Alamo et al., 2011). Our data suggests that in the absence of NAC, SRP interacts with such nascent chains and can interfere with their biogenesis. SRP and Ssb1/2 were recently shown to interact with distinct nascent chain clients (Willmund et al., 2013). Hence, it is likely that in the absence of NAC, SRP interferes with Ssb1/2 function, leading to cytosolic protein aggregation. This is entirely consistent with the close match in aggregation profile observed in *Δssb1/2Δnac* and *nac* mutants overexpressing SRP shown in this study. We detected the strongest phenotype upon SRP overexpression in the *Δegd1* mutant, consistent with the previous observation that Egd1 preferentially associates with cytoplasmic proteins (del Alamo et al., 2011).

We revisited the role of NAC in cotranslational translocation and find that at 16°C, or when SRP levels are limiting as in a *sec65-1* mutant, translocation of Pho8 is inefficient when NAC is compromised. These defects appear to be specifically linked to the Egd2 subunit, as *Δegd2* mutants show SRP-dependent, but not Sec62-dependent translocation defects, whereas *Δegd1* cells have no defect in either pathway.

SRP levels are greatly substoichiometric to ribosomes (Raue et al., 2007), and this is further exacerbated in the *sec65-1* cells. Under these conditions, the time window before signal sequence recognition can occur is likely to be extended. If unchecked, this would increase the likelihood of SRP-dependent substrates aggregating as they are intrinsically hydrophobic. Hence, a potential function for Egd2 would be to prevent aggregation before signal sequence recognition. Entirely consistent with this hypothesis, *sec65-1* strains accumulate detergent-insoluble aggregates of newly synthesized proteins, including the SRP-dependent precursor Pho8, and this is exacerbated by simultaneous deletion of Egd2. In contrast, overexpression of Egd2 reduces aggregation of Pho8 and partially rescues translocation of SRP-dependent precursors.

These observations are consistent with the recent results observed in *C. elegans*, identifying a chaperone function for NAC (Kirstein-Miles et al., 2013). The aggregates observed in the *sec65-1* were ubiquitinated, and this was reduced upon expression of Egd2. This correlates with a previous study that showed that NAC protects nascent chains from cotranslational ubiquitination (Duttler et al., 2013).

NAC was previously shown to exist predominantly as a heterodimer of Egd2 and Egd1 (Reimann et al., 1999). However, the αNAC homologue from archaea forms a homodimer (Spreter et al., 2005). Moreover, studies in yeast showed that Egd2 alone, specifically associates with secretory nascent chains, consistent with a role for the Egd2 homodimer in the biogenesis of secretory proteins (del Alamo et al., 2011).

In the absence of Egd1, Egd2 associated with the ribosome, albeit at a reduced level and resulted in a 52-kD adduct upon cross-linking, which is entirely consistent with the size of an Egd2 homodimer. Furthermore, this cross-link was increased upon Egd2 overexpression and was also detected with purified Egd2. The Egd2 homodimer was also detected under native conditions, suggesting that separate pools of homo- and heterodimers are associated with ribosomes in vivo. The presence of native Egd2 complexes in the size range of 48 to 68 kD (Reimann et al., 1999) in the *Δ*egd1 strain is also in agreement with the presence of an Egd2 homodimer. However, previous studies suggested that Egd2 is less likely to homodimerize in the presence of Egd1 (Spreter et al., 2005). Consistent with this, levels of the homodimer were very low in the WT strain.

Collectively, our data indicate that NAC modulates the interaction of SRP with the ribosome, as suggested previously (Powers and Walter, 1996), and this in turn influences binding of additional ligands such as Map1. In the presence of NAC, SRP can bind to the ribosome such that Map1 can also be accommodated (Fig. 7). The fact that SRP makes multiple contacts with ribosome (six in the case of canine SRP; Halic et al., 2004) may permit an initial low-affinity binding conformation that utilizes only a subset of these contacts. This conformation would be compatible with the presence of NAC and other ligands such as Map1.

Secretory chains first contact NAC, and then subsequently SRP54 (Wiedmann et al., 1994; Jungnickel and Rapoport, 1995; Zhang et al., 2012), hence NAC may act to preserve a "sampling mode" whereby multiple factors can bind the ribosome simultaneously (Holtkamp et al., 2012). This would allow Map1 to bind and process N termini as well as permitting sampling of the nascent chain by SRP. Subsequent signal sequence-recognition by SRP would then lead to the release of NAC (Fig. 7), permitting SRP to make extensive ribosome contacts (Zhang et al., 2012), which are no longer compatible with Map1 binding. These two modes of interaction of SRP with the ribosome are consistent with the changes in the Sec65 cross-linking profile observed when SRP is overexpressed in strains lacking βNAC as compared with WT strain.

The presence of a signal sequence inside the ribosome exit tunnel was shown to increase the affinity of SRP for ribosomes (Berndt et al., 2009). This may occur by subtly altering the arrangement of the ribosome and/or NAC at the exit site such that SRP binding is more favored. This might then facilitate more efficient delivery of the signal sequence to SRP. It is conceivable that these changes could favor binding of the Egd2 homodimer over the Egd1/Egd2 heterodimer.

Our data suggest Egd2 can prevent aggregation of secretory nascent chains when SRP is at reduced levels. In the absence of SRP, in vitro studies show that probes within the signal sequence of RNC readily cross-link to NAC (Jungnickel and Rapoport, 1995). Hence in the sampling mode, NAC may also function to prevent aggregation of the signal sequence before SRP's arrival.

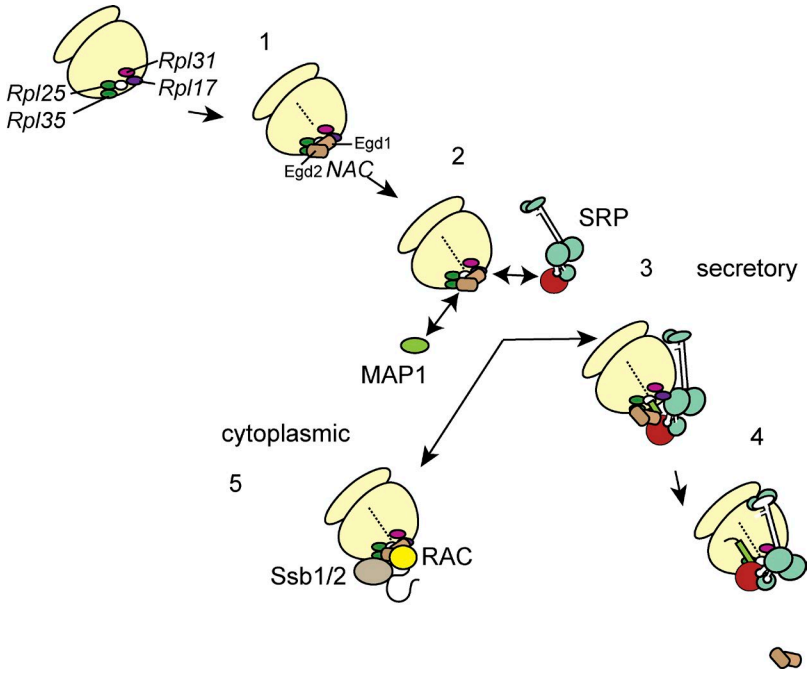

Figure 7. **Model indicating a novel role for NAC in regulating the access of MAP and SRP to the ribosome.** Short nascent chains first encounter NAC, which interacts with the ribosome close to Rpl25/35 and Rpl31/17 (1). The presence of NAC allows both SRP and Map1 to bind the ribosome and sample nascent chains (2). The presence of an SRP substrate changes the conformation of NAC, possibly in response to a signal sequence/anchor in the exit tunnel such that SRP can bind the signal sequence (3). The α subunit of NAC can prevent aggregation of the signal sequence before the arrival of SRP. Handover of the signal sequence to SRP releases NAC leading to tight binding of SRP (4). Nonsecretory proteins interact with RAC and Ssb1/2 as the nascent chain extends (5). In the absence of NAC, SRP binding precludes Map1 binding thereby compromising processing and folding of cytosolic proteins.

Materials and methods

Yeast strains, culture, and genetic manipulation

Yeast strains were grown either in YPD (rich) media (1% [wt/vol] yeast extract, 2% [wt/vol] peptone, and 2% [wt/vol] glucose) or minimal media (0.67% [wt/vol] yeast nitrogen base and 2% [wt/vol] glucose) plus appropriate amino acids supplements. All yeast strains were cultured at 30°C, unless otherwise specified. Standard yeast protocols were used for transformations (Guthrie and Fink, 1991).

S. cerevisiae strains used in this study are listed in Table S1. Unless indicated otherwise, the WT and single knockout strains were obtained from the BY4741 series of the EUROSCARF strain collection (Winzeler et al., 1999). Double-deletion strains were constructed by mating, diploid sporulation, and dissection of haploids as previously described (Guthrie and Fink, 1991). YNY1 was constructed by mating *Δegd2* and *sec65-1* strains and YNY2 was constructed by mating *Δegd1* and *Δbtt1*. In brief, diploid yeast strains were constructed by mixing haploid strains of opposite mating types on YPD solid medium. After incubating overnight, diploids were positively selected on YNB solid medium using appropriate auxotrophic markers. Diploid strains were grown to stationary phase at 30°C, in presporulation medium (0.8% [wt/vol] yeast extract, 0.3% [wt/vol] Bacto-peptone) supplemented with 10% (wt/vol) glucose after autoclaving. Cells were washed with sterile ddH_2O and resuspended in 10 ml of sporulation medium (1% [wt/vol] potassium acetate, 0.1% [wt/vol] Yeast extract) containing appropriate amino acid and supplements at a final concentration of 0.002% (wt/vol) and 0.05% (wt/vol) glucose. Sporulation was allowed to proceed by growing at 24°C for 3–4 d, after which the efficiency of sporulation was monitored microscopically. Once sufficient sporulation had occurred, 10 µl of cells were diluted with 190 µl of ddH_2O and treated with 5 units of Zymolyase T100 (AMS Biotechnology Ltd) for 5 min. Next, 10 µl of the treated spores were run vertically down a YPD solid medium plate and allowed to dry. A Narishige micro-manipulator microscope was used to separate the four spores from each ascus. This was performed upon a minimum of 10 complete tetrads. Spores were allowed to grow on YPD solid medium at 30°C for 2–3 d. Haploid progeny of dissections were tested for gene deletion by the presence of G418-Geneticin cassette, growth at 37°C, and Western blotting for absence of different NAC subunits.

RS453, *RPL25GFP*, and *Δmap1* (GFY9) strains were C-terminally tagged with 3x HA at the *MAP2* locus using a cassette amplified from the pYM24 (using gene-specific primers; Table S2), which confers resistance to the antibiotic Hygromycin B to the transformed yeast (Janke et al., 2004). The HA-tagging was confirmed by both PCR and Western blot analysis.

Plasmid construction

Plasmids used in this study are listed in Table S3, and the primers for constructing plasmids and strains are listed in Table S2. Plasmids construction was performed using standard molecular biology techniques.

The MAP1 ORF, ∼1,400 bp including 500 bp of 5′ sequence, was amplified from genomic DNA using primers Map1FLAGF and Map1 FLAGR and then ligated into pMP220 (Dalley et al., 2008) cut with SalI and PstI. The resulting plasmid, pMP289, drives Map1FLAG expression under its own endogenous promoter and the *NUF2* 3′UTR. To generate the plasmid for overexpressing Map1 under the high copy glyceraldehyde-3-phosphate dehydrogenase promoter, the entire ORF was amplified by PCR from yeast genomic DNA using primers Map1F and Map1R, which include flanking BamHI and EcoRI sites, respectively. The resulting ∼1,164-bp fragment was digested with these same enzymes and ligated into BamHI and EcoRI digested pRS414-GPD (Mumberg et al., 1995). The resulting plasmid, pMP299, encodes the complete *MAP1* ORF expressed from the strong GPD promoter.

The Map2 open reading frame was amplified from genomic DNA with primers Map2HAF and Map2HAR, which add a C-terminal triple-HA tag and flanking BamHI and EcoRI sites. The resulting fragment was then cloned into pRS414GPD via these restriction sites to give pMP305.

To generate the plasmid for overexpressing Egd1, the entire ORF was amplified by PCR from yeast genomic DNA using primers EGD1F and EGD1R that include flanking PstI and NotI sites, respectively. The resulting ∼1,480-bp fragment was digested with these same enzymes and ligated into PstI and NotI digested pRS422 (2µ) vector (Sikorski and Hieter, 1989). The resulting plasmid, pMP300, encodes the complete *EGD1* under the control of the endogenous promoter. To generate the plasmid for overexpressing Egd2, the entire *EGD2* ORF was amplified by PCR from yeast genomic DNA using primers EGD2F and

EGD2R, which included flanking SalI and PstI sites, respectively. The resulting ~975-bp fragment was digested with these same enzymes and ligated into SalI and PstI sites digested pRS412 (CEN) and pRS422 (2μ) vectors (Sikorski and Hieter, 1989), yielding plasmids, pMP301 and pMP302, respectively. To generate the plasmid for overexpressing NAC, the PCR products for *EGD1* and *EGD2* were digested as described above and were both cloned into the same vector pRS412 (CEN) and pRS422 (2μ) to give plasmids pMP304 and pMP303, respectively. To overexpress Egd2 in *E. coli* with a cleavable N-terminal his-tag, the *EGD2* ORF was amplified from pMP301 using primers EGD2pET28F and EGD2pET28R, which include flanking NdeI and BamHI sites and was ligated into pET28 digested with NdeI and BamHI to yield pMP306.

Subcellular fractionation: ribosome pelleting

Yeast cells were grown in complete media to an OD_{600} of ~0.6, and then treated with 0.1 mg/ml cycloheximide for 10 min. Cells were resuspended in lysis buffer (100 mM KOAc, 20 mM Hepes-KOH, 5 mM $Mg[OAc]_2$, 4 mM DTT, 0.1 mg/ml cycloheximide, 1 mM PMSF, and Roche protease inhibitors) and broken by glass bead lysis and resulting cells lysates cleared of cellular debris by centrifugation at 1,200 *g*. Membranes were solubilized by the addition of 1% (wt/vol) CHAPS, in the presence of 100 mM KOAc (low salt) or variable salt concentrations as indicated up to 500 mM KOAc (high salt). Insoluble material was removed by centrifugation for 20 min at 16,000 *g*. The resulting supernatant was centrifuged for 1 h at 256,000 *g,* through a 500-mM sucrose cushion in lysis buffer, to generate a ribosome-enriched pellet and post-ribosomal supernatant.

Polysome analysis

To fractionate the polyribosomes, 5 OD_{260nm} units of lysate were applied to the top of a 13-ml linear 10–55% (wt/vol) sucrose gradient in lysis buffer and centrifuged for 150 min at 285,000 *g* at 4°C in a SW40 rotor (Beckman). Gradients were fractionated using ISCO gradient fractionator with continuous monitoring of A_{260nm} to detect monosomes and polysome peaks.

Mass spectrometry

Coomassie-stained bands were excised from gels, reduced, and then alkylated before digestion with trypsin. Digested samples were analyzed by LC-MS/MS using a NanoAcquity LC (Waters) coupled to a LTQ Velos (Thermo Fisher Scientific). Peptides were concentrated on a precolumn (20 mm × 180 μm i.d., Waters), and then separated using a gradient from 99% A (0.1% [vol/vol] formic acid in water) and 1% B (0.1% (vol/vol) formic acid in acetonitrile) to 30% B, in 40 min at 300 nl/min^{-1}, using a 75 mm × 250 μm i.d. 1.7 μM BEH C18, analytical column (Waters). Peptides were selected for fragmentation automatically by data-dependent analysis.

Chemical cross-linking

Ribosome-enriched pellet fractions were resuspended in lysis buffer (100 mM KOAc; in the absence of DTT when using MBS and GMBS) at a concentration of 32 OD_{260}/ml and incubated with DSS, MBS, or GMBS at a final concentration of 100–500 μM (prepared as a 20 mM stock in DMSO) for 10 min at 25°C before quenching with 10 mM glycine pH 7.5/10 mM 2-mercaptoethanol.

In vivo pulse-labeling and denaturing immunoprecipitation

WT or knockout yeast cells were grown in YNB medium with appropriate supplements to an OD_{600} of ~0.2. Where indicated, cells were grown in the presence of 10 μg/ml tunicamycin (Merck) for 90 min before labeling. Pulse-labeling was initiated by addition of 10 μCi of [^{35}S] methionine/cysteine cell labeling mix (Perkin-Elmer) per OD_{600nm} units of cells for 5–10 min at 30°C (20 min at 16°C). Labeling was terminated by addition of ice cold sodium azide to a final concentration of 20 mM. For each sample, 10 OD_{600nm} units of cells were harvested. Radiolabeled yeast cells were then spheroplasted with Zymolyase 100T (AMS Biotechnology) before addition of lysis buffer (1% SDS, 50 mM Tris-HCl, pH 7.4, and 5 mM EDTA), and then incubated at 95°C for 5 min. Samples were then diluted with 5 volumes of immunoprecipitation buffer (62.5 mM Tris-HCl, pH 7.4, 1.25% (vol/vol) Triton X-100, 190 mM NaCl, and 6.25 mM EDTA), precleared with protein A beads for 1 h, and then anti-Dap2 antisera added to the supernatant. After 1 h, immune complexes were recovered by adding protein A Sepharose and incubating for another hour, followed by washing three times before elution with SDS-PAGE sample buffer. Samples were analyzed by SDS-PAGE and visualized by phosphorimaging. In the case of unlabeled cells the same protocol was used following cross-linking and anti-HA (Roche) or FLAG resins (Sigma) were used for immunoprecipitation

Isolation of aggregated proteins

Isolation of aggregated proteins from yeast mutants was performed as previously described (Koplin et al., 2010). In brief, cells were grown to 0.6 OD_{600} units in minimal medium with appropriate selection. Cells were harvested, and resulting cell pellets were resuspended in lysis buffer (20 mM Na-phosphate, pH 6.8, 10 mM DTT, 1 mM EDTA, 0.1% [vol/vol] Tween 20, 1 mM PMSF, protease inhibitor cocktail [Roche], 3 mg/ml zymolyase 100T, and 1.25 U/ml benzonase) and incubated at room temperature for 20 min. Chilled samples were treated by tip sonication and centrifuged for 20 min at 200 g at 4°C. Supernatants were adjusted to same OD_{280nm}, and aggregated proteins were pelleted at 16,000 *g* for 20 min at 4°C. After removing supernatants, aggregated proteins were washed twice with 2% (vol/vol) NP-40 (in 20 mM Na-phosphate, pH 6.8, 1 mM PMSF, and protease inhibitor cocktail), sonicated again, and centrifuged again at 16,000 *g* for 20 min at 4°C. Aggregated proteins were washed in NP-40–deficient buffer, sonicated, boiled in SDS sample buffer, separated by SDS-PAGE (14%), and analyzed by Coomassie staining.

PNGase F treatment

Deglycosylation of protein was performed by digesting isolated aggregates or precleared lysates with PNGase F. In brief, isolated aggregates or total lysate were solubilized in 1X Glycoprotein Denaturing Buffer (New England Biolabs) in a 10 μl total reaction volume. Samples were denatured by heating the reaction mix to 100°C for 10 min. Next, 2 μl of 10× G7 Reaction Buffer, 2 μl of 10% (vol/vol) NP-40, 2 μl PNGase F (New England Biolabs), and 4 μl of water were added. The reaction was incubated at 37°C for 1 h. Analysis was carried out by SDS-PAGE and Western blotting.

Translocation reporter assays

To monitor translocation, *PHO8-URA3* (cotranslational) and *CPY-URA3* (posttranslational) reporter-based assays were performed as described previously (Dalley et al., 2008). In brief, yeast cells transformed with reporter plasmids pMP234 *(PHO8-URA3)* and pMR12 *(CPY-URA3)* were streaked in parallel on minimal media plates lacking either leucine alone or both uracil and leucine, and then grown at either 16°C or 30°C for 2–5 d. Growth in the absence of uracil is indicative of a defect in translocation.

MetAP enzymatic assay

The methionine aminopeptidase activity of total cell lysates was monitored by using the fluorescent based assay as previously described (Li et al., 2003). Extracts were prepared in a buffer containing 50 mM MOPS, pH 7.0, 5 mM $Mg(OAc)_2$, and 5 mM $CoCl_2$ as the divalent cat-

ion. The reaction was initiated by the addition of 100 µM Met-AMC. The cleavage of the Met from Met-AMC (I-1265.0250; Bachem) was monitored by measuring the release of AMC by fluorescence spectroscopy (Em wavelength of 460 nm with Ex wavelength at 360 nm).

Protein expression

The His-tagged Egd2 protein was expressed in *E. coli* BL21(DE3) and purified via nickel-nitrilotriacetic acid-agarose (QIAGEN; according to the manufacturer's manual). The His tag was removed from Egd2 by thrombin cleavage during the purification procedure.

Image acquisition

Radioactive gels were imaged using a Typhoon FLA-7000 phosphorimager (GE Healthcare) and subsequently processed using Aida software (Raytest). ECL films (BioMX MR; Kodak), Coomassie-stained gels and plates were scanned with an Epson Perfection V700 using Image Capture (Apple) or Adobe Photoshop software. Coomassie-stained gels were quantified using Aida (Raytest). Statistical analysis was performed with GraphPad (Prism).

Antibodies

Anti-myc (mouse, 4A6) was obtained from Upstate; anti-HA (mouse, HA-7), anti-FLAG M2 (mouse), and anti-Zwf1p (rabbit) were purchased from Sigma-Aldrich; and Pho8 antibody (mouse, 1D3A10) was purchased from Life Technologies. Antibodies against Rps3p (rabbit, peptide VALISKKRKLVADC$_{CONH2}$), Rpl35p (rabbit, peptide CPIRKYAIKV$_{COOH}$), Rpl25p, DPAP B, CPY, Sec65p, Egd1p, and Egd2p have been described previously (Stirling et al., 1992; Ogg et al., 1998; Mason et al., 2000; Frey et al., 2001; Panasenko et al., 2006) Antibodies to Map1 and Rpl17 were raised in rabbits (Cambridge Research Biochemicals) against the epitopes CARNKKSPGGPRQRIK-$_{COOH}$ and [C]-Ahx-QVNQAPKQRRRTYR-CONH$_2$, respectively.

Online supplemental material

Table S1 shows yeast strains. Table S2 shows primers used in the study. Table S3 lists plasmids used in the study. Fig. S1 shows analysis of ribosomes from *prt1-1* and *rpl25GFP* strains. Fig. S2 shows that Map1 and Egd2 are both adjacent to Rpl35 when bound to the ribosome. Fig. S3 shows cross-link analysis of ribosome-associated Egd1 and Egd2. Fig. S4 shows that overexpression of SRP in *egd1* and *egd2* mutant strains retards growth and reduces MetAP activity. Fig. S5 shows that overexpression of Egd1 and Egd2 leads to distinct SRP-dependent translocation phenotypes. Online supplemental material is available at http://www.jcb.org/cgi/content/full/jcb.201410086/DC1.

Acknowledgment

We thank Mark Ashe, Martine Collart, Jesús de la Cruz, Elke Deuerling, Sabine Rospert, Blanche Schwappach, Lu Jingping, and Colin Stirling for strains and reagents. We thank Elena Martín-Rodríguez for generation of the Map1$_{FLAG}$ plasmid, Barrie Wilkinson for assistance with tetrad dissection, and Chris Grant for critical comments on the manuscript. Mass spectrometry was performed by the Biomolecular Analysis Core Facility (University of Manchester, Manchester, England, UK).

This work was supported by grants from the BBSRC [H007202/1] and Wellcome Trust [097820/Z/11/A].

The authors declare no competing financial interests.

Submitted: 23 October 2014
Accepted: 3 June 2015

References

Akopian, D., K. Shen, X. Zhang, and S.O. Shan. 2013. Signal recognition particle: an essential protein-targeting machine. *Annu. Rev. Biochem.* 82:693–721. http://dx.doi.org/10.1146/annurev-biochem-072711-164732

Ban, N., R. Beckmann, J.H. Cate, J.D. Dinman, F. Dragon, S.R. Ellis, D.L. Lafontaine, L. Lindahl, A. Liljas, J.M. Lipton, et al. 2014. A new system for naming ribosomal proteins. *Curr. Opin. Struct. Biol.* 24:165–169. http://dx.doi.org/10.1016/j.sbi.2014.01.002

Becker, T., S. Bhushan, A. Jarasch, J.P. Armache, S. Funes, F. Jossinet, J. Gumbart, T. Mielke, O. Berninghausen, K. Schulten, et al. 2009. Structure of monomeric yeast and mammalian Sec61 complexes interacting with the translating ribosome. *Science.* 326:1369–1373. http://dx.doi.org/10.1126/science.1178535

Berndt, U., S. Oellerer, Y. Zhang, A.E. Johnson, and S. Rospert. 2009. A signal-anchor sequence stimulates signal recognition particle binding to ribosomes from inside the exit tunnel. *Proc. Natl. Acad. Sci. USA.* 106:1398–1403. http://dx.doi.org/10.1073/pnas.0808584106

Boissel, J.P., T.J. Kasper, and H.F. Bunn. 1988. Cotranslational amino-terminal processing of cytosolic proteins. Cell-free expression of site-directed mutants of human hemoglobin. *J. Biol. Chem.* 263:8443–8449.

Dalley, J.A., A. Selkirk, and M.R. Pool. 2008. Access to ribosomal protein Rpl25p by the signal recognition particle is required for efficient cotranslational translocation. *Mol. Biol. Cell.* 19:2876–2884. http://dx.doi.org/10.1091/mbc.E07-10-1074

del Alamo, M., D.J. Hogan, S. Pechmann, V. Albanese, P.O. Brown, and J. Frydman. 2011. Defining the specificity of cotranslationally acting chaperones by systematic analysis of mRNAs associated with ribosome-nascent chain complexes. *PLoS Biol.* 9:e1001100. http://dx.doi.org/10.1371/journal.pbio.1001100

Duttler, S., S. Pechmann, and J. Frydman. 2013. Principles of cotranslational ubiquitination and quality control at the ribosome. *Mol. Cell.* 50:379–393. http://dx.doi.org/10.1016/j.molcel.2013.03.010

Forte, G.M., M.R. Pool, and C.J. Stirling. 2011. N-terminal acetylation inhibits protein targeting to the endoplasmic reticulum. *PLoS Biol.* 9:e1001073. http://dx.doi.org/10.1371/journal.pbio.1001073

Frey, S., M. Pool, and M. Seedorf. 2001. Scp160p, an RNA-binding, polysome-associated protein, localizes to the endoplasmic reticulum of *Saccharomyces cerevisiae* in a microtubule-dependent manner. *J. Biol. Chem.* 276:15905–15912. http://dx.doi.org/10.1074/jbc.M009430200

Gilmore, R., G. Blobel, and P. Walter. 1982. Protein translocation across the endoplasmic reticulum. I. Detection in the microsomal membrane of a receptor for the signal recognition particle. *J. Cell Biol.* 95:463–469. http://dx.doi.org/10.1083/jcb.95.2.463

Gloge, F., A.H. Becker, G. Kramer, and B. Bukau. 2014. Co-translational mechanisms of protein maturation. *Curr. Opin. Struct. Biol.* 24:24–33. http://dx.doi.org/10.1016/j.sbi.2013.11.004

Guthrie, C., and G.R. Fink. 1991. Molecular Enzymology: Guide to Yeast Genetics and Molecular Cell Biology. Academic Press, London.

Halic, M., and R. Beckmann. 2005. The signal recognition particle and its interactions during protein targeting. *Curr. Opin. Struct. Biol.* 15:116–125. http://dx.doi.org/10.1016/j.sbi.2005.01.013

Halic, M., T. Becker, M.R. Pool, C.M. Spahn, R.A. Grassucci, J. Frank, and R. Beckmann. 2004. Structure of the signal recognition particle interacting with the elongation-arrested ribosome. *Nature.* 427:808–814. http://dx.doi.org/10.1038/nature02342

Holtkamp, W., S. Lee, T. Bornemann, T. Senyushkina, M.V. Rodnina, and W. Wintermeyer. 2012. Dynamic switch of the signal recognition particle from scanning to targeting. *Nat. Struct. Mol. Biol.* 19:1332–1337. http://dx.doi.org/10.1038/nsmb.2421

Huang, S., R.C. Elliott, P.S. Liu, R.K. Koduri, J.L. Weickmann, J.H. Lee, L.C. Blair, P. Ghosh-Dastidar, R.A. Bradshaw, K.M. Bryan, et al. 1987. Specificity of cotranslational amino-terminal processing of proteins in yeast. *Biochemistry.* 26:8242–8246. http://dx.doi.org/10.1021/bi00399a033

Hurt, E., S. Hannus, B. Schmelzl, D. Lau, D. Tollervey, and G. Simos. 1999. A novel in vivo assay reveals inhibition of ribosomal nuclear export in ran-cycle and nucleoporin mutants. *J. Cell Biol.* 144:389–401. http://dx.doi.org/10.1083/jcb.144.3.389

Jackson, R., and T. Hunter. 1970. Role of methionine in the initiation of haemoglobin synthesis. *Nature.* 227:672–676. http://dx.doi.org/10.1038/227672a0

Janke, C., M.M. Magiera, N. Rathfelder, C. Taxis, S. Reber, H. Maekawa, A. Moreno-Borchart, G. Doenges, E. Schwob, E. Schiebel, and M. Knop. 2004. A versatile toolbox for PCR-based tagging of yeast genes: new fluorescent proteins, more markers and promoter substitution cassettes. *Yeast.* 21:947–962. http://dx.doi.org/10.1002/yea.1142

Jungnickel, B., and T.A. Rapoport. 1995. A posttargeting signal sequence recognition event in the endoplasmic reticulum membrane. *Cell.* 82:261–270. http://dx.doi.org/10.1016/0092-8674(95)90313-5

Kirstein-Miles, J., A. Scior, E. Deuerling, and R.I. Morimoto. 2013. The nascent polypeptide-associated complex is a key regulator of proteostasis. *EMBO J.* 32:1451–1468. http://dx.doi.org/10.1038/emboj.2013.87

Koplin, A., S. Preissler, Y. Ilina, M. Koch, A. Scior, M. Erhardt, and E. Deuerling. 2010. A dual function for chaperones SSB-RAC and the NAC nascent polypeptide-associated complex on ribosomes. *J. Cell Biol.* 189:57–68. http://dx.doi.org/10.1083/jcb.200910074

Leidig, C., G. Bange, J. Kopp, S. Amlacher, A. Aravind, S. Wickles, G. Witte, E. Hurt, R. Beckmann, and I. Sinning. 2013. Structural characterization of a eukaryotic chaperone—the ribosome-associated complex. *Nat. Struct. Mol. Biol.* 20:23–28. http://dx.doi.org/10.1038/nsmb.2447

Li, X., and Y.H. Chang. 1995. Amino-terminal protein processing in *Saccharomyces cerevisiae* is an essential function that requires two distinct methionine aminopeptidases. *Proc. Natl. Acad. Sci. USA.* 92:12357–12361. http://dx.doi.org/10.1073/pnas.92.26.12357

Li, J.Y., L.L. Chen, Y.M. Cui, Q.L. Luo, J. Li, F.J. Nan, and Q.Z. Ye. 2003. Specificity for inhibitors of metal-substituted methionine aminopeptidase. *Biochem. Biophys. Res. Commun.* 307:172–179. http://dx.doi.org/10.1016/S0006-291X(03)01144-6

Martinez, A., J.A. Traverso, B. Valot, M. Ferro, C. Espagne, G. Ephritikhine, M. Zivy, C. Giglione, and T. Meinnel. 2008. Extent of N-terminal modifications in cytosolic proteins from eukaryotes. *Proteomics.* 8:2809–2831. http://dx.doi.org/10.1002/pmic.200701191

Mason, N., L.F. Ciufo, and J.D. Brown. 2000. Elongation arrest is a physiologically important function of signal recognition particle. *EMBO J.* 19:4164–4174. http://dx.doi.org/10.1093/emboj/19.15.4164

Mumberg, D., R. Müller, and M. Funk. 1995. Yeast vectors for the controlled expression of heterologous proteins in different genetic backgrounds. *Gene.* 156:119–122. http://dx.doi.org/10.1016/0378-1119(95)00037-7

Naranda, T., S.E. MacMillan, and J.W. Hershey. 1994. Purified yeast translational initiation factor eIF-3 is an RNA-binding protein complex that contains the PRT1 protein. *J. Biol. Chem.* 269:32286–32292.

Ng, D.T., J.D. Brown, and P. Walter. 1996. Signal sequences specify the targeting route to the endoplasmic reticulum membrane. *J. Cell Biol.* 134:269–278. http://dx.doi.org/10.1083/jcb.134.2.269

Nissen, P., J. Hansen, N. Ban, P.B. Moore, and T.A. Steitz. 2000. The structural basis of ribosome activity in peptide bond synthesis. *Science.* 289:920–930. http://dx.doi.org/10.1126/science.289.5481.920

Nyathi, Y., B.M. Wilkinson, and M.R. Pool. 2013. Co-translational targeting and translocation of proteins to the endoplasmic reticulum. *Biochim. Biophys. Acta.* 1833:2392–2402. http://dx.doi.org/10.1016/j.bbamcr.2013.02.021

Ogg, S.C., W.P. Barz, and P. Walter. 1998. A functional GTPase domain, but not its transmembrane domain, is required for function of the SRP receptor beta-subunit. *J. Cell Biol.* 142:341–354. http://dx.doi.org/10.1083/jcb.142.2.341

Panasenko, O., E. Landrieux, M. Feuermann, A. Finka, N. Paquet, and M.A. Collart. 2006. The yeast Ccr4-Not complex controls ubiquitination of the nascent-associated polypeptide (NAC-EGD) complex. *J. Biol. Chem.* 281:31389–31398. http://dx.doi.org/10.1074/jbc.M604986200

Pech, M., T. Spreter, R. Beckmann, and B. Beatrix. 2010. Dual binding mode of the nascent polypeptide-associated complex reveals a novel universal adapter site on the ribosome. *J. Biol. Chem.* 285:19679–19687. http://dx.doi.org/10.1074/jbc.M109.092536

Pechmann, S., F. Willmund, and J. Frydman. 2013. The ribosome as a hub for protein quality control. *Mol. Cell.* 49:411–421. http://dx.doi.org/10.1016/j.molcel.2013.01.020

Peisker, K., D. Braun, T. Wölfle, J. Hentschel, U. Fünfschilling, G. Fischer, A. Sickmann, and S. Rospert. 2008. Ribosome-associated complex binds to ribosomes in close proximity of Rpl31 at the exit of the polypeptide tunnel in yeast. *Mol. Biol. Cell.* 19:5279–5288. http://dx.doi.org/10.1091/mbc.E08-06-0661

Powers, T., and P. Walter. 1996. The nascent polypeptide-associated complex modulates interactions between the signal recognition particle and the ribosome. *Curr. Biol.* 6:331–338. http://dx.doi.org/10.1016/S0960-9822(02)00484-0

Preissler, S., and E. Deuerling. 2012. Ribosome-associated chaperones as key players in proteostasis. *Trends Biochem. Sci.* 37:274–283. http://dx.doi.org/10.1016/j.tibs.2012.03.002

Raue, U., S. Oellerer, and S. Rospert. 2007. Association of protein biogenesis factors at the yeast ribosomal tunnel exit is affected by the translational status and nascent polypeptide sequence. *J. Biol. Chem.* 282:7809–7816. http://dx.doi.org/10.1074/jbc.M611436200

Reimann, B., J. Bradsher, J. Franke, E. Hartmann, M. Wiedmann, S. Prehn, and B. Wiedmann. 1999. Initial characterization of the nascent polypeptide-associated complex in yeast. *Yeast.* 15:397–407. http://dx.doi.org/10.1002/(SICI)1097-0061(19990330)15:5<397::AID-YEA384>3.0.CO;2-U

Sandikci, A., F. Gloge, M. Martinez, M.P. Mayer, R. Wade, B. Bukau, and G. Kramer. 2013. Dynamic enzyme docking to the ribosome coordinates N-terminal processing with polypeptide folding. *Nat. Struct. Mol. Biol.* 20:843–850. http://dx.doi.org/10.1038/nsmb.2615

Sikorski, R.S., and P. Hieter. 1989. A system of shuttle vectors and yeast host strains designed for efficient manipulation of DNA in Saccharomyces cerevisiae. *Genetics.* 122:19–27.

Sin, N., L. Meng, M.Q. Wang, J.J. Wen, W.G. Bornmann, and C.M. Crews. 1997. The anti-angiogenic agent fumagillin covalently binds and inhibits the methionine aminopeptidase, MetAP-2. *Proc. Natl. Acad. Sci. USA.* 94:6099–6103. http://dx.doi.org/10.1073/pnas.94.12.6099

Spreter, T., M. Pech, and B. Beatrix. 2005. The crystal structure of archaeal nascent polypeptide-associated complex (NAC) reveals a unique fold and the presence of a ubiquitin-associated domain. *J. Biol. Chem.* 280:15849–15854. http://dx.doi.org/10.1074/jbc.M500160200

Starheim, K.K., K. Gevaert, and T. Arnesen. 2012. Protein N-terminal acetyltransferases: when the start matters. *Trends Biochem. Sci.* 37:152–161. http://dx.doi.org/10.1016/j.tibs.2012.02.003

Stirling, C.J., and E.W. Hewitt. 1992. The *S. cerevisiae SEC65* gene encodes a component of yeast signal recognition particle with homology to human SRP19. *Nature.* 356:534–537. http://dx.doi.org/10.1038/356534a0

Stirling, C.J., J. Rothblatt, M. Hosobuchi, R. Deshaies, and R. Schekman. 1992. Protein translocation mutants defective in the insertion of integral membrane proteins into the endoplasmic reticulum. *Mol. Biol. Cell.* 3:129–142. http://dx.doi.org/10.1091/mbc.3.2.129

Vetro, J.A., and Y.H. Chang. 2002. Yeast methionine aminopeptidase type 1 is ribosome-associated and requires its N-terminal zinc finger domain for normal function in vivo. *J. Cell. Biochem.* 85:678–688. http://dx.doi.org/10.1002/jcb.10161

Voorhees, R.M., I.S. Fernández, S.H. Scheres, and R.S. Hegde. 2014. Structure of the mammalian ribosome-Sec61 complex to 3.4 Å resolution. *Cell.* 157:1632–1643. http://dx.doi.org/10.1016/j.cell.2014.05.024

Wegrzyn, R.D., D. Hofmann, F. Merz, R. Nikolay, T. Rauch, C. Graf, and E. Deuerling. 2006. A conserved motif is prerequisite for the interaction of NAC with ribosomal protein L23 and nascent chains. *J. Biol. Chem.* 281:2847–2857. http://dx.doi.org/10.1074/jbc.M511420200

Wiedmann, B., H. Sakai, T.A. Davis, and M. Wiedmann. 1994. A protein complex required for signal-sequence-specific sorting and translocation. *Nature.* 370:434–440. http://dx.doi.org/10.1038/370434a0

Willmund, F., M. del Alamo, S. Pechmann, T. Chen, V. Albanèse, E.B. Dammer, J. Peng, and J. Frydman. 2013. The cotranslational function of ribosome-associated Hsp70 in eukaryotic protein homeostasis. *Cell.* 152:196–209. http://dx.doi.org/10.1016/j.cell.2012.12.001

Winzeler, E.A., D.D. Shoemaker, A. Astromoff, H. Liang, K. Anderson, B. Andre, R. Bangham, R. Benito, J.D. Boeke, H. Bussey, et al. 1999. Functional characterization of the S. cerevisiae genome by gene deletion and parallel analysis. *Science.* 285:901–906. http://dx.doi.org/10.1126/science.285.5429.901

Xu, H., and M.A. Freitas. 2009. MassMatrix: a database search program for rapid characterization of proteins and peptides from tandem mass spectrometry data. *Proteomics.* 9:1548–1555. http://dx.doi.org/10.1002/pmic.200700322

Zhang, Y., U. Berndt, H. Gölz, A. Tais, S. Oellerer, T. Wölfle, E. Fitzke, and S. Rospert. 2012. NAC functions as a modulator of SRP during the early steps of protein targeting to the endoplasmic reticulum. *Mol. Biol. Cell.* 23:3027–3040. http://dx.doi.org/10.1091/mbc.E12-02-0112